Simultaneous UV Direct Writing of Channel Waveguides and Bragg Gratings in Germanium-Doped Planar Silica

Paulo V. S. Marques, Jim R. Bonar, António M. P. Leite, and J. S. Aitchison

***Abstract*—Channel waveguides incorporating photo-imprinted Bragg gratings were produced in germano-borosilicate glass layers fabricated by flame hydrolysis deposition, through single- and double-step exposure direct writing processes with UV laser irradiation. To our knowledge, this is the first time that UV exposure has been used to simultaneously realize both waveguiding and spectral selectivity functions.**

***Index Terms*—Bragg gratings, direct writing, flame hydrolysis, integrated optics, optical devices, photosensitivity.**

I. Introduction

THE flame hydrolysis deposition technique was developed to synthesize high-purity fine silica particles, employing a method of vapor delivery and its subsequent hydrolysis in a high-temperature flame, using an oxy-hydrogen torch [1]. Its high throughput, excellent doped silica quality, and extreme versatility in terms of doping species led Kawachi *et al.* [2] to apply flame hydrolysis deposition (FHD) to the realization of planar lightwave circuits (PLCs). Since this first work, numerous results have been published confirming FHD, in conjunction with reactive ion etching, as a very performant technique in this PLC domain. In addition, the FHD process has been used to produce rare-earth-doped waveguide lasers and amplifiers in silica [3]. However, one of the limiting steps in producing an integrated circuit is the reactive ion etching step which is both costly and time consuming. Attention is therefore beginning to focus on the use of photosensitivity as a method for transferring the waveguide pattern into the silica glass.

Over the last decade, there has been a great research effort directed at the exploitation of photosensitivity in optical fibers and planar waveguides, stimulated by the extremely important role of the resulting devices in optical communication and sensing systems. The photosensitivity effect has been used primarily to produce in-core Bragg gratings using the permanent index change obtained under UV exposure [4], [5], but it can also be usefully employed in UV trimming of devices [6], [7] and in direct writing of two-dimensional (2-D) devices, such as directional couplers [8], [9] and power splitters [9]. Direct writing is particularly attractive since it avoids recourse to reactive ion etching (RIE) in defining the waveguide structures.

In this paper, simultaneous photo-imprinting of a straight waveguide with a Bragg grating along its central section is reported. The results obtained indicate that the fabrication of more elaborate devices, such as WDMs based on grating technology (add–drop filters) [10], should be entirely feasible using this technique. We begin by reviewing the FHD process for the production of germanium-doped silica. This will be followed by detailed descriptions of the experiments carried out with a view of realizing a 2-D waveguide with a Bragg grating.

Manuscript received September 3, 2002; revised October 2, 2002.

P. V. S. Marques is with the INESC PORTO, Optoelectronics and Electronics Systems Unit, 4169-007 Porto, Portugal. He is also with the Departamento de Física, Faculdade de Ciências, Universidade do Porto, 4169-007 Porto, Portugal (e-mail: psmarque@fc.up.pt).

J. R. Bonar is with Alcatel Optronics UK Limited, Livingston, EH54 8SF U.K.

A. M. P. Leite is with the Departamento de Física, Faculdade de Ciências, Universidade do Porto, 4169-007 Porto, Portugal.

J. S. Aitchison is with the Edward S. Rogers Sr. Department of Electrical and Computer Engineering, University of Toronto,Toronto, ON M5S 3G4, Canada.

Digital Object Identifier 10.1109/JSTQE.2002.806730

II. Experiment

A. The FHD System

In this section we review the basic FHD process used to deposit photosensitive glass compositions. The FHD system used in this work incorporates a reagents cabinet, which consists of a sealed glove box that contains the bubbler bottles with their respective reagents ($SiCl_4$, $POCl_3$, and $GeCl_4$). The carrier gas (N_2) flow is guaranteed through high-precision mass flow controllers (MFCs) and its flow path is determined by pneumatic bellow valves, whose configuration permits the bypass of nitrogen through the reagent bottles and adjustment of the individual flow rates while in a stand-by situation. Since this method relies on a vapor delivery technique, for good feeding control the reagents are kept at a constant temperature by silicone oil circulating in a closed circuit through the outer jacket of their respective reagent Drechels bottles. BCl_3 was already supplied as a gas and therefore used a separated delivery line.

The hydrolysis reaction takes place in the closed deposition chamber (at atmospheric pressure) which houses the circular turntable where the substrates are placed and the oxy-hydrogen torch. Two computer-controlled stepper motors are assembled underneath the chamber, one used for turntable rotation and the other for the linear movement of the arm that holds the torch. The final thickness of the glass layer deposited is determined by the combined movements of rotation of the turntable with linear displacement of the torch above the substrates. A local exhaust is placed above the turntable surface in order to ensure an efficient removal of corrosive reaction products and unreacted reagents.

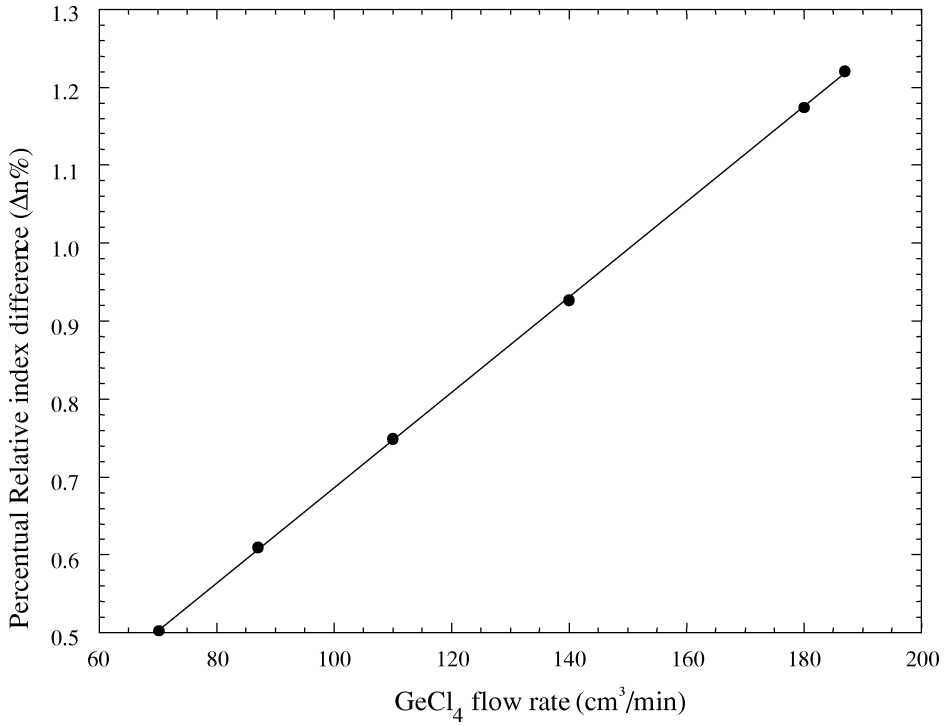

Fig. 1. Flame hydrolysis deposition system calibration for germano-borosilicate glass. The $SiCl_4$ and BCl_3 flow rates were 150 and 65 cm^3/min, respectively. The oxygen and hydrogen flow rates were 7 and 5 l/min, respectively.

Calibration of the FHD system was first conducted using planar waveguides; the most important characteristic parameters to be determined are the thickness and the refractive index of the slab layer versus dopants concentration, as well as the optimal sintering conditions required to achieve defect-free glass layers.

Several parameters were investigated, such as reagent flow, flame and turntable temperature, torch position, and sintering parameters (dwell temperature and time, temperature ramps and sintering environment). In all cases the flame was fed with constant flow rates for $SiCl_4$ (150 cm^3/min) and BCl_3 (65 cm^3/min), while the $GeCl_4$ flow rate was adjusted in order to control the refractive index difference to the thermal oxide layer. Flame fueling was ensured by constant flows of O_2 (5 l/min) and H_2 (7 l/min), as a more efficient incorporation of germanium was found with high-temperature flames, probably due to better reaction efficiency. The samples were sintered in a tubular furnace in a helium-rich environment produced by a constant helium flow of 0.6 l/min. The sintering temperature was approximately 1325 °C for a dwell time of 2.5 h. The samples were inserted and removed at approximately 850 °C and the ramping rates employed were 15 °C/min. Fig. 1 shows the result of the refractive index characterization as a function of the $GeCl_4$ flow rate, which is relevant for the deposition of core layers. The refractive index of the planar layer was measured using the m-lines technique. The parameters employed resulted in a final layer thickness of 1.0 ± 0.1 μm per pass of the torch.

B. Photosentivity Assessment

Following FHD system calibration, the first topic addressed in this study was the characterization of the photosensitive response of germanium-boron-doped silica produced by FHD. Two methods were adopted to measure the increase in the refractive index as a function of preprocessing (i.e., hydrogenation) and UV exposure parameters.

In the first method, the refractive index changes in planar waveguides due to UV exposure were determined by protecting half of the sample while uniformly exposing the other half. The changes were determined by comparing the refractive index of both areas, as given by the prism coupler and m-lines technique. Due to the absence of a cladding layer, flame brushing employing an oxy-hydrogen torch [11] was used as the photosensitization method (flame brushing induces permanent hydrogenation as opposed to "cold" hydrogenation at high pressure, where molecular hydrogen will rapidly diffuse out).

In the second method, Bragg gratings were written into standard channel waveguides to determine the photosensitive response. In this case, the core layer was deposited on preoxidized silicon wafers using FHD; the samples were then patterned and the waveguide cores defined using RIE techniques. The channel waveguides were then buried using a cladding layer, with the refractive index matching that of the thermal silicon dioxide buffer. Gratings were photo-imprinted using the conventional phase mask approach, with phase masks fabricated in-house using e-beam writing techniques and RIE applied to fused silica plates. Analysis of the characteristics of the Bragg gratings obtained and their interpretation according to conventional methods resulted in the extraction of the relevant induced refractive index changes and of the process dynamics.

The saturation values for index change in planar waveguides (core thickness of 6 μm and relative refractive index difference of $\Delta n/n = 0.75\%$) due to UV exposure, using a KrF excimer

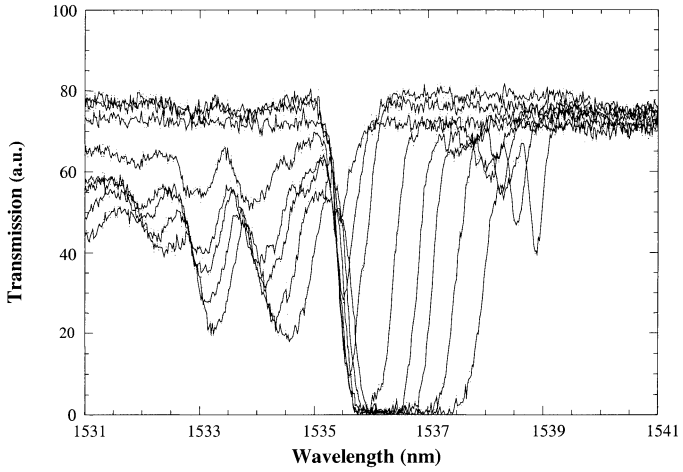

Fig. 2. Evolution of the Bragg grating transmission spectrum with UV exposure (200 mJ/cm^2 per pulse at 20 Hz). The narrowest and the broadest spectra were obtained with 4500 and 35 000 pulses, respectively.

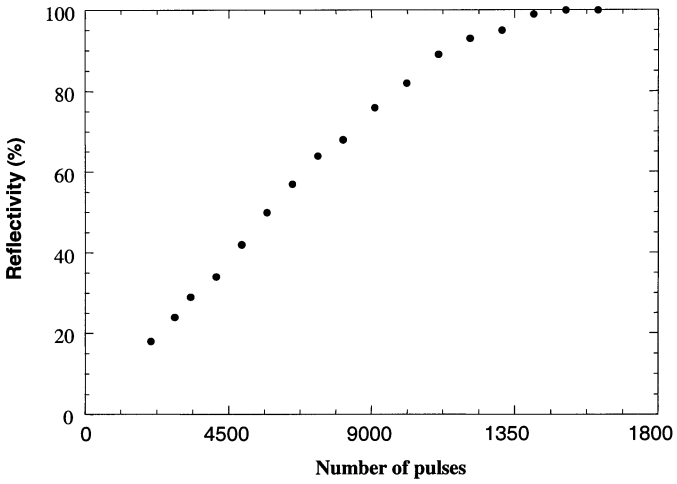

Fig. 3. Evolution of peak reflectivity for the grating characterized in Fig. 2.

laser operating at 248 nm, were 5×10^{-4} for as-grown samples and 4×10^{-3} for flame-brushed samples. The transmission spectrum evolution due to UV exposure through a 6-mm-long phase mask (period of 1060 nm) in an etched waveguide with a relative refractive index contrast to the thermal buffer layer of 0.75% and core dimensions of 6×6 μm^2 can be seen in Fig. 2. The samples were hydrogen loaded prior to UV exposure for ~ 2 weeks in a high-pressure chamber (120 atm, room temperature). Analysis of the evolution of the grating spectral characteristics shows that the central Bragg wavelength moves toward longer wavelengths as the exposure proceeds, due to an increase of the average core refractive index. Simultaneously, there is an increase of the grating bandwidth and side features start to develop as the exposure progresses toward saturation. There is a characteristic rise in coupling to higher order modes that reflects itself on a drop in transmission at wavelengths shorter than the central Bragg wavelength. The peak that develops at a longer wavelength is attributed to e-beam writing stitching errors in the phase mask used.

Fig. 3 shows the evolution of the maximum grating reflectivity as a function of the UV exposure; this behavior is characteristic of FHD germanium-doped silica, which exhibits a positive refractive index change due to exposure. The refractive index change estimated from the results of Figs. 2 and 3 is a rise of at least 3.6×10^{-3}. When the samples are exposed under, or close to, a saturation condition, higher order grating effects were observed, including multiple reflection peaks due to multimode operation of the waveguide at shorter wavelengths (Fig. 4).

These results indicate that values of refractive index change sufficient to induce 2-D confinement in planar structures are achievable. Therefore, experiments were subsequently conducted to demonstrate simultaneous writing of channel waveguides and Bragg gratings.

C. Channel Waveguide Writing

To evaluate the capability of writing channel waveguides, the layered planar structure shown in Fig. 5 was employed. The central photosensitive layer, doped with germanium and boron, had a thickness d_1 of 6 μm and a relative index difference of 0.9% with respect to the thermal oxide lower cladding. The core was covered with a $d_o = 15$ μm thick layer doped with phosphorous and boron, its refractive index matching that of the buffer layer; this cover layer was designed to be transparent at the writing wavelength, and its thickness was chosen to simultaneously permit a reasonable hydrogen retention time after removal from the hydrogenation chamber, and an attempt to avoid diffraction effects as reported in [4]. The amplitude mask deposited on top of the upper-cladding was fabricated by nichrome thermal evaporation, followed by a photolithographic process and nichrome wet-etching. The process is similar to that employed with standard etched waveguides, although the amplitude mask for UV direct writing is obviously the negative of the mask used for dry-etching of standard waveguides. Another approach involved amplitude masks defined on UV grade silica plates, which were put in contact with the sample surface, with the mask facing down. This would in principle reduce the fabrication time, since a single mask could be used for more than one sample, but the method is more sensitive to mechanical vibrations (which are minimized by pressing down the mask against the sample with strong clamps specially designed to the effect). The devices were treated with the same hydrogenation routine as the samples used for grating tests. The top view of a set of straight waveguides defined by direct writing is shown in Fig. 6. Diffraction effects are not to be seen, and the waveguide dimensions clearly reproduce quite well the mask widths. One negative point of this method is that the metallic mask can be damaged by the UV exposure. The threshold for damage was determined to be approximately 300 mJ/cm^2 per pulse at 30 Hz for masks on transparent silica plates; in the case of nichrome masks deposited on the sample surface, the threshold for mask damage seemed to be smaller. In the former case, UV radiation hits the mask interface in contact with the fused silica, which is obviously very clean and nonoxidized. In the case of NiCr layers deposited on the sample surface, the UV light exposes the surface layers that are not so clean and probably oxidized, and this is possibly a cause for the lower threshold for damage. In Fig. 7(a), the photograph of a sample (top view) with severe NiCr damage is presented for illustration; at the points of NiCr

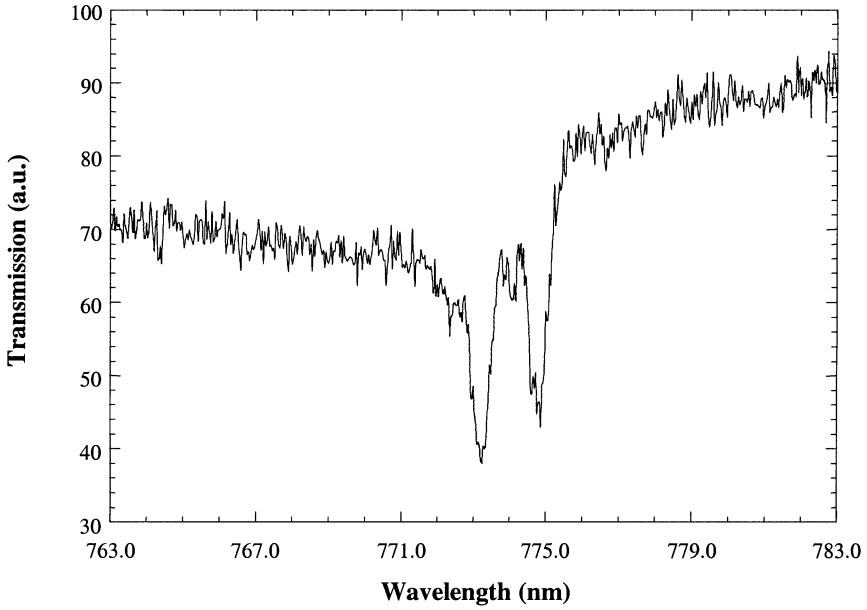

Fig. 4. Transmission spectrum of the second order of the Bragg grating characterized in Fig. 2 after 35 000 pulses.

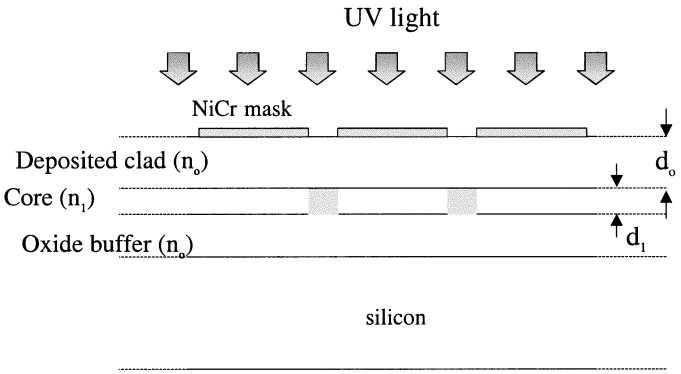

Fig. 5. Schematic representation of the cross-section structure of the samples used for direct writing experiments.

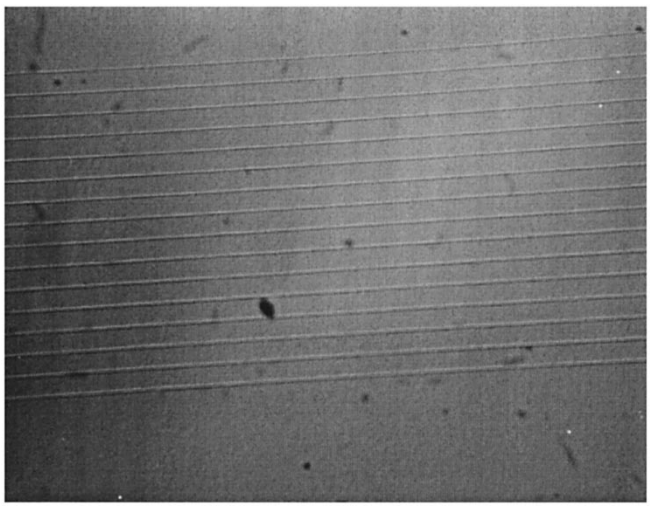

Fig. 6. Top view of a set of directly written straight waveguides with widths ranging from 3 to 18 μm (250 mJ/cm^2 per pulse, 25 Hz, 15 min).

breakdown, the sample is exposed through the fractures, this being clearly visible in Fig. 7(b) after NiCr removal.

D. Channel Waveguide Bragg Gratings

The use of photosensitivity to obtain optical guidance by refractive index modification, together with a superimposed refractive index modulation to form a Bragg waveguide grating, was then investigated. In the first approach, samples were exposed to a focused KrF excimer laser beam, operating at 248 nm, through a nonabsorbing fused silica plate in contact with the sample surface and containing, in its central section, a 6-mm-long phase mask with a period of 1060 nm. The laser beam was focused into a straight line, orthogonal to the phase mask grooves, using a cylindrical lens. The focused line was long enough to expose the whole sample length in a single step, avoiding the need for any kind of high-precision beam scanning.

The sample was exposed to a UV fluence of 200 mJ/cm^2 per pulse at 40 Hz, for a duration of 15 min. A straight waveguide with a Bragg grating along its central part was obtained. A periodic core modulation, with the same period of the phase mask, was clearly observable under an optical microscope, indicating that the grating was of type II. As a result, several higher orders of the grating could be observed in the transmission spectrum of the straight waveguide, as shown in Fig. 8. Due to the large modulation in the refractive index, there was a considerable amount of coupling to cladding modes, especially near the second-order peak wavelength of the grating at 1546 nm (index matching fluid over the cladding modified these resonances). Losses due to OH-absorption were also observable around 1400 nm. In this experiment, the focused laser line was ~ 50 μm, and resulted in multimode waveguide operation. We measured an insertion loss of 4.4 dB at 1100 nm. This result was obtained in an 11-mm-long sample, using a single-mode fiber at the input and a multimode fiber in the output.

In the second approach, the sample surface was coated with an 80-nm-thick film of nichrome. Using photolithography and wet-etching, lines with widths ranging from 3 to 10 μm

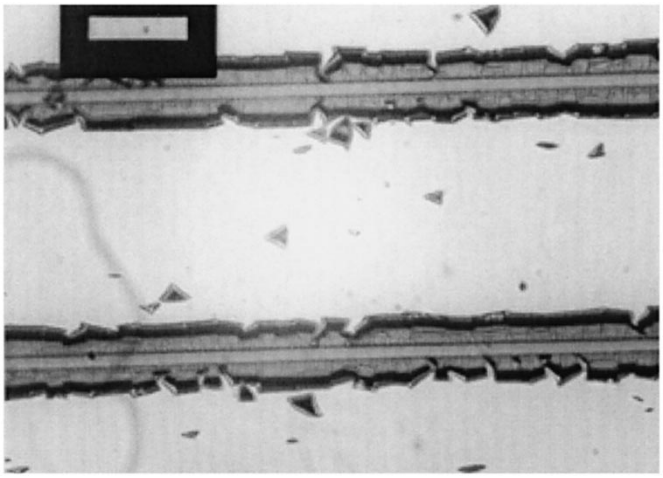

(a)

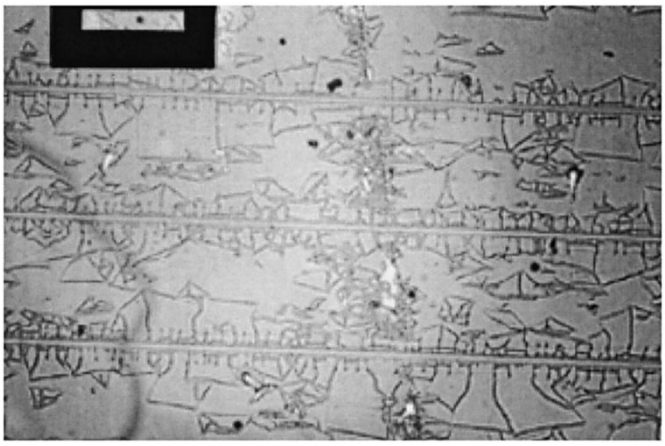

(b)

Fig. 7. (a) Damage of the mask defined on an 80-nm-thick NiCr layer deposited on the sample (325 mJ/cm^2 per pulse, 30 Hz, 15 min). (b) Top view of the sample after NiCr removal (325 mJ/cm^2 per pulse, 30 Hz, 15 min).

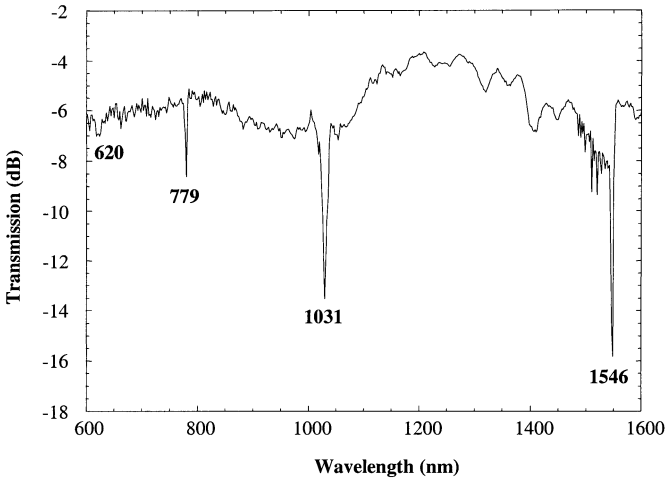

Fig. 8. Transmission spectrum of a directly written linear waveguide with a Bragg grating obtained under simultaneous UV exposure.

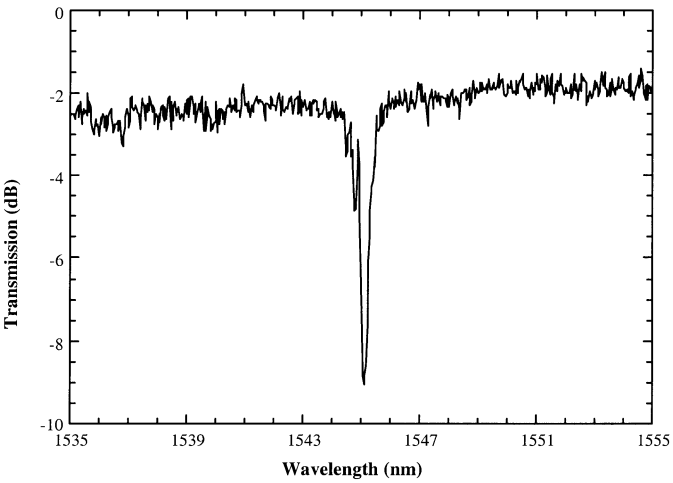

Fig. 9. Grating in directly written single-mode waveguide obtained by a double-exposure process.

were defined in the nichrome mask. Exposure proceeded in two-steps; in the first, the sample was evenly exposed, through the mask, to the UV beam, without phase mask (7 min, 20 Hz, 200 mJ/cm^2 per pulse), for definition of a homogeneous "background" waveguide, and care was taken in order to avoid saturation of the refractive index change. Exposure was then stopped, and a phase mask was placed in contact with the sample surface and aligned with the nichrome mask. A second exposure step was then performed to define a Bragg grating in the channel waveguide "predefined" in the first exposure (additional 12 min exposure, 20 Hz, 200 mJ/cm^2 per pulse). The result is shown in Fig. 9, where a $\sim$80% reflectivity grating in a single-mode waveguide was obtained. The central Bragg wavelength shifted to longer wavelengths in this case, because the effective index in directly written waveguides was higher than in the etched waveguides referred above. The short wavelength resonances recorded in this case can also be due to a nonuniform UV exposure. This situation usually results in a nonconstant refractive index average along the grating length that leads to a symmetrically chirped Bragg grating, causing Fabry–Pérot interference effects to develop in the transmission spectrum.

The exposure time for each exposure step was roughly calculated from the growth dynamics shown in Fig. 3, and the objective was to attain a 100% reflectivity grating after the second exposure. Several factors can be responsible for the lower reflectivity achieved. The growth dynamics used in the calculation was obtained from gratings in channel waveguides with a relative index difference of 0.75%, instead of an etched channel waveguide with the same refractive index difference as the photosensitive layer normally used for direct writing (0.9%). There is the possibility of differing growth dynamics, dependent on the GeO_2 concentration, and hence misadjustement of the exposure times in the new situation. Two possibilities can occur: too much exposure in the first step, leaving only a small refractive index change to be attainable in the second step and, consequently, making a 100% reflectivity grating impossible to be obtained even if saturation is reached; alternatively, the exposure dose in the second step was not sufficient. However, the first hypothesis is the most plausible one, since the Bragg gratings grow faster for higher germanium concentrations for similar exposure doses. The phase mask substrate employed was longer than the

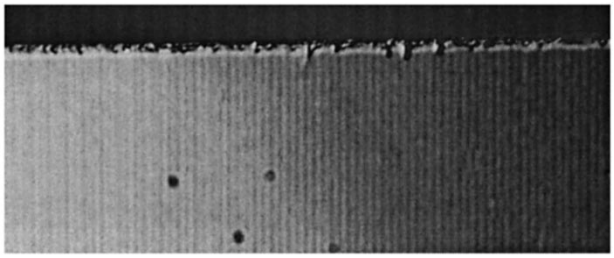

Fig. 10. Effects of UV exposure through the phase mask on the nichrome film. The period of the "groove" effect in the nichrome film is equal to the period of the phase mask.

device, and thus allowed the entire sample to be exposed but eliminated the possibility of fiber butt-coupling (and hence of real time monitoring of grating growth).

The refractive index change was, in this case, extrapolated from the position of the central Bragg wavelength. Calculations were performed for a 6×6 μm^2 core with a refractive index $n^{\text{core}} + \Delta n^{\text{UV}}$. For $\lambda_B = 1545$ nm, the refractive index change was calculated to be $\Delta n^{\text{UV}} \sim 6 \times 10^{-3}$ (for a relative index difference of the photosensitive layer to the adjacent layers of 0.9%). The insertion loss measured in the same waveguide was 4.5 dB, using single-mode fibers (mode field diameter of 10.5 μm at $1/e$). The calculated coupling loss was approximately 2 dB per endfacet, and thus the estimated propagation loss was 0.5 dB/cm.

A very positive aspect of simultaneous writing of waveguide plus grating is that, from the central Bragg wavelength (which is directly related to the modal effective index constant) and from the waveguide dimensions, it is possible to accurately extract the UV induced refractive index simply by employing a mode solver like the effective index method. A negative point in this approach is the occurrence of damage in the nichrome mask; Fig. 10 shows a microphotograph of the sample after exposure. In this picture, a periodic effect in the nichrome film is clearly seen (with the same period of the phase mask), probably due to annealling effects induced by the UV light. On the nichrome line edges, it is possible to observe some irregularities due to mask erosion, which are thought to be responsible for the high propagation losses reported. In previous experiments on direct writing of simple waveguides through nichrome masks, the threshold for damage was determined to be 300 mJ/cm^2 at 30 Hz (free beam). When a phase mask is used, the fluence increases at locations of construtive interference, and hence the threshold, as measured in the free beam, is reduced, but this fact was not considered in the calculation of the UV fluence level.

III. Conclusion

The photosensitive response of germanium-boron-doped silica obtained by FHD on oxidised silicon substrates was characterized in this study. Additionally, demonstration of direct writing of both monomode and multimode 2-D waveguides with a Bragg grating using two different exposure processes was conducted. This was a first step toward a practical method for mass production of elaborate devices avoiding dry-etch processing steps. Insertion losses can be reduced either by using a matched refractive index structure as described in [12] and by lower UV fluence levels avoiding nichrome mask degradation.

Acknowledgment

The authors thank Dr. X. Liu for supplying some of the e-beam written phase masks used on this work.

References

[1] J. F. Hyde, "Method of Making a Transparent Article of Silica," U.S. Patent 2 272 342, Feb. 10, 1942.

[2] M. Kawachi, M. Yasu, and T. Edahiro, "Fabrication of SiO_2 – TiO_2 glass planar optical waveguides by flame hydrolysis deposition," *Electron. Lett.*, vol. 19, no. 15, pp. 583–584, 1983.

[3] J. R. Bonar and J. S. Aitchison, "Co-doping effects in rare earth doped planar waveguides," *Proc. Inst. Elect. Eng.—Optoelectronics*, vol. 143, pp. 293–297, 1996.

[4] V. Mizrahi, P. J. Lemaire, T. Erdogan, T. Erdogan, W. A. Reed, and D. J. Digiovanni, "Ultraviolet laser fabrication of ultrastrong optical fiber gratings and of germania-doped channel waveguides," *Appl. Phys. Lett.*, vol. 63, no. 13, pp. 1727–1729, 1993.

[5] G. D. Maxwell, R. Kashyap, B. J. Ainslie, D. L. Williams, and J. R. Armitage, "UV written 1.5 μm reflection filters in single mode planar silica guides," *Electron. Lett.*, vol. 28, no. 22, pp. 2106–2107, 1992.

[6] R. A. Jarvis, J. D. Love, and F. Ladouceur, "Bend-radius reduction in planar waveguides using UV post-tuning," *Electron. Lett.*, vol. 33, no. 10, pp. 892–894, 1997.

[7] R. Kashyap, G. D. Maxwell, and B. J. Ainslie, "Laser-trimmed four-port bandpass filter fabricated in single-mode photosensitive Ge-doped planar waveguide," *IEEE Photon. Technol. Lett.*, vol. 5, pp. 191–194, Feb. 1993.

[8] G. D. Maxwell and B. J. Ainslie, "Demonstration of directly written directional coupler using UV induced photosensitivity in a planar silica waveguide," *Electron. Lett.*, vol. 31, no. 2, pp. 95–96, 1995.

[9] M. Svalgaard, "Direct writing of planar waveguide power splitters and directional couplers using a focused ultraviolet laser beam," *Electron. Lett.*, vol. 33, no. 20, pp. 1694–1695, 1997.

[10] T. Erdogan, T. A. Strasser, M. A. Milbrodt, E. J. Laskowski, C. H. Henry, and G. E. Kohnke, "Integrated-optical Mach-Zehnder add-drop filter fabricated by a single UV-induced grating exposure," *Appl. Opt.*, vol. 36, no. 30, pp. 7838–7845, 1997.

[11] F. Bilodeau, B. Malo, J. Albert, D. C. Jonhson, K. O. Hill, Y. Hibino, M. Abe, and M. Kawachi, "Photosensitization in optical fiber and silica on silicon/silica waveguides," *Opt. Lett.*, vol. 18, no. 12, pp. 953–955, 1993.

[12] D. Zauner, K. Kulstad, J. Rathje, and M. Svalgaard, "Directly UV-written silica-on-silicon planar waveguides with low insertion loss," *Electron. Lett.*, vol. 34, no. 16, pp. 1582–1584, 1998.

Paulo V. S. Marques was born in Coruche, Portugal, in 1968. He received the degree in physics, the M.Sc. degree in optoelectronics and lasers, and the Ph.D. degree in physics, all from the University of Porto, Porto, Portugal, in 1991, 1995, and 2000, respectively.

His Ph.D. research program was conducted under a strong collaboration with the Department of Electronics and Electrical Engineering of the University of Glasgow, and it involved the development of passive and active integrated optical devices using flame hydrolysis deposition. He also actively participated in other research projects involving ion-exchange, lithium-niobate-based devices, and polymer waveguides. In November 1999 he was appointed as Teaching Assistant at University of Trás-os-Montes e Alto Douro, Portugal, and was promoted to Assistant Professor in November 2000. In 2001, he joined the Faculty of Science of the University of Porto as an Assistant Professor. Since July 2000, his research activity has been focused on the Optoelectronics and Electronics Systems Unit of INESC PORTO, which is responsible for several National and European research contracts. His current research interests include hybrid sol-gel-based waveguides, optical photosensitivity, Bragg gratings, electric field poling, optical switching, and integrated optical sensors.

Jim R. Bonar received the Ph.D. degree from the University of Glasgow, Glasgow, U.K., in 1995.

Subsequently, he held the position of Research Associate and then Lecturer. In 1997, he was awarded a Fellowship from the Royal Society of Edinburgh/ SE. In 1998, he joined the start-up company Kymata Ltd. The company develops and manufactures passive optical components. Since joining the company, he has worked as a Technology Manager, Product Manager and R&D Chief Process Engineer. He is now Director of Product Technology for Alcatel Optronics UK Ltd., Livingston, U.K. During his career he has worked on rare-earth-doped silica waveguide amplifiers and lasers, polymer waveguides, multimode structures for sensing applications, and Si micromachining. He has authored and coauthored six patent applications and approximately 30 journal and conference papers.

António M. P. Leite received the degree in electrical engineering from the University of Porto, Porto, Portugal, in 1973 and received the Ph.D. degree from University College London, London, U.K., in 1979. His doctoral research focused on holographic optical elements.

He was appointed an Associate Professor with the Department of Physics, University of Porto, in 1979 and since then has been involved in projects on optical communication, fiber sensors, and integrated optic devices in lithium niobate, III-V semiconductors, polymers, and glass. His current interests are in the field of integrated optics (glass and polymer devices, electrooptic and rare-earth-doped devices), fiber sensors, and sensor networks.

J. S. Aitchison, photograph and biography not available at the time of publication.